Contents lists available at ScienceDirect

Materials Science in Semiconductor Processing

Review article

Deterministic doping

CrossMark

David N. Jamieson*, William I.L. Lawrie, Simon G. Robson, Alexander M. Jakob,
Brett C. Johnson, Jeffrey C. McCallum

ARC Centre for Quantum Computation and Communication Technology, School of Physics, University of Melbourne, Parkville, Victoria 3010, Australia

A R T I C L E   I N F O

A B S T R A C T

Emerging programs in a new field of technology that employs quantum mechanical principles in engineered devices has driven new approaches to atomic-scale fabrication. Of crucial importance is the capability to configure single atoms in silicon, diamond and other materials. These engineered materials form the foundations of quantum technology which includes the fields of quantum communication and quantum computing. Quantum technology exploits quantum superposition and entanglement in potentially scalable quantum devices. To insert donor atoms in a large-scale device methods for deterministic ion implantation have been developed. These methods potentially allow the standard techniques developed for engineering materials for the Information Technology industry to be employed to make devices that exploit the new technologies. This paper reviews the emerging new technologies for deterministic doping to address the challenges of engineering atoms in the solid state.

1. Introduction

The second quantum revolution, as described by Dowling [1], is the development of new technologies employing quantum mechanics that has now emerged as a significant field of research. These technologies include quantum computing [2–4], quantum cryptography [5], quantum simulation [6,7], quantum metrology [8,9], quantum sensing in biology [10] or geology [11], quantum time keeping [12], quantum imaging [13] and the quantum internet [14]. There has been significant progress in the development of devices based on the new field of silicon quantum electronics [15] or photonics [16]. In the case of solid state devices employing nuclear or electron spins [17] based on silicon [18] or diamond [19] large scale devices will require the precision engineering of single dopant atoms or colour centres in a crystalline matrix. Ion implantation is already highly developed for silicon in the information technology industry [20] and significant progress has been made towards employing ion implantation to build devices engineered with single atoms in silicon and other materials [21]. For the fabrication of arrays of one or more single atoms the technique of deterministic ion implantation has been developed where implantation is done in conjunction with a method for the registration of each implanted ion.

Recent demonstrations of electron and nuclear spin control of single phosphorus dopant atoms implanted into silicon have shown single donor spin qubits in silicon are strong contenders in the quest for the realization of a scalable quantum computer device [22–25]. The

next step of demonstrating reliable two qubit coupling is likely achievable with existing technology but for this to be achieved on a larger scale requires new techniques for building atomic arrays of implanted donors into silicon including deterministic ion implantation. Also, although much of the present focus is on phosphorus, the heavy donor atoms of arsenic, antimony and bismuth can be implanted into a silicon lattice at a given depth with higher spatial resolution due their higher mass (see Table 1). Also, in the case of arsenic and antimony, diffusion in silicon is less affected by oxidation enhanced diffusion [28] and hence potentially offers higher placement precision compared to phosphorus considering the need for post-implant annealing steps. In the case of antimony the donor electron Bohr orbit diameter is larger than the other donors [26] which may serve to relax constraints on construction precision. Implantation of heavy donor atoms into silicon will cause significant lattice damage, but it has been shown that an ultra-scaled CMOS device can withstand the implantation of erbium isotopes ($161 < A < 171$, comparable to bismuth: A=209) where the optically excited charge and spin state of a single implanted erbium atom was detected electrically [29]. Also bismuth donor electron spin resonance can be successfully measured in ensembles implanted into silicon [30]. A potential new application beyond spin qubits in the case of bismuth donors in silicon arises from the fact that the donor electron exhibits technologically useful clock transitions which are insensitive to external perturbations [31]. This transition has so far only been studied in ensembles not in single donors. This demonstrates that ion

---

* Corresponding author.
  E-mail address: d.jamieson@unimelb.edu.au (D.N. Jamieson).

Table 1
Characteristics of implanted donors in Si and C. Bohr orbit data adapted from [26], implantation data from [27], energy per e-h pair in Si 3.6 eV [82], diamond 13.2 eV [83]. In each case the proportion of the initial ion energy that contributes to the production of e-h pairs is close to 40%.

Matrix: Donor	Bohr orbit diameter (nm)	Energy (keV)	Mean implantation depth (nm)	Lateral straggling (nm)	Number of e-h pairs per impact
C(diamond): N	–	15	20	6.3	710
Si: P	2.44	13	20	9	1600
Si: P	2.44	8	15	7	900
Si: As	1.96	20	20	7	2100
Si: Sb	2.64	22	20	5	2250
Si: Er	–	25	20	5	2700
Si: Bi	1.94	26	20	4	2900

implantation into wafer scale arrays of fully fabricated and encapsulated devices is a robust method for the introduction of single and few ions and it can be expected that this will also be true for dopant arrays.

2. Materials and methods

By placing single arsenic, antimony and bismuth atoms in arrays, it is possible, at low temperatures, to configure the local electrostatic landscape of the device for manipulation of the associated donor electrons and through spin-orbit coupling, also the donor nuclear spins. Magnetoelectric transport through single donors is affected by the donor electron level structure, which depends on the dopant-specific properties. Some of these applications employ standard analytical spectroscopic techniques of high source-drain voltage bias [32] and electrically detected magnetic resonance (EDMR) spectroscopy [33]. Devices that exploit these methods have already been used to demonstrate the hybrid classical-quantum technology needed for single spin readout such as: (i) the coupling of a single phosphorus [25,34,35], arsenic [36–38] or antimony [39,40] donor to a silicon-based single-electron transistor (SET) or field effect transistor, (ii) spin dependent scattering from antimony ensembles [41], (iii) the coupling of a small ensemble of donor spins to the 2-dimensional electron gas (2DEG) in an accumulation-mode silicon MOSFET [33,42], and (iv) the strong coupling of a Cooper pair box dipole [43] (capacitive-coupling) or an ensemble of electron spins (magnetic-coupling) in either silicon [44], ruby [45] or in diamond using the NV- centres [46,47] to a superconducting transmission-line resonator. These methods have now also been applied to acceptor atoms including boron in silicon [48]. A review [49] presents other applications of single atom doping for applications to new device technologies including single-dopant transistors and photonic devices employing a single dopant atom as a functional component.

2.1. Fabrication methods

This extensive collection of measurements on single atom devices represents the state-of-the-art and justifies the next step of using deterministic methods for fabrication of scaled devices beyond single donors. In the present review we confine our attention to ion implantation. This is because, in many cases, ion implantation is also

compatible with the process flow for the fabrication of ultra-scaled devices. Also, as shown in Fig. 1, the limiting precision imposed by ion straggling for a donor implanted 20 nm deep in silicon can be as low as 4 nm for bismuth (see Table 1) which is promising for devices incorporating large-scale arrays. The simulations in Fig. 1 neglect the effect of ion channelling which is known to result in deep, low concentration, tails in the ion distribution. Studies of 14 keV P implanted ion profiles with atom probe tomography reveals [50] approximately 20% of the ions are deeper than the simulations for ions implanted through a native surface oxide. Implantation through a prefabricated gate oxide is likely to suppress the channelling tail to some extent.

For ion implantation to be useful in the construction of single-atom arrays, a deterministic ion implantation signal is required to register single ions either before they impact with the substrate or after impact making use of a signal from the substrate. In the case of pre-impact techniques, these can employ especially configured ion sources which provide one ion at a time to the implanter [51,52] or by pre-assembling an array of ions in a magnetic optical trap [53,54]. In some of these systems the ion source can produce very cold beams allowing the ions to be focused to ~6 nm precision which is an advantage for using a scanned beam to implant large scale arrays [55]. However, as yet these advanced ion sources are not yet readily compatible with the required dopants for silicon.

In the case of post-implant techniques, it is possible to employ several different signals from the substrate. For example, by using secondary electron emission as the implant signal in a focused ion beam microscope it was possible to implant counted 60 keV phosphorus [56], silicon [57] and arsenic [58] ions into silicon devices with an aiming precision around 60 nm. One of the factors that degrades the spatial precision of the implantation is ion straggling (see Table 1). This can be reduced with lower implantation energies. However, it is possible the secondary electron yield will also be lower which could reduce the reliability of the signal. By using higher charge state ions, it is possible to recover this signal and this technique has been used with highly charged antimony and bismuth ions [59].

An alternative signal from the substrate that can be used to count ion implantation events is to employ pre-fabricated ultra-scaled field effect transistors in which the source drain current is sensitive to the damage created by the passage of a single ion through the transistor
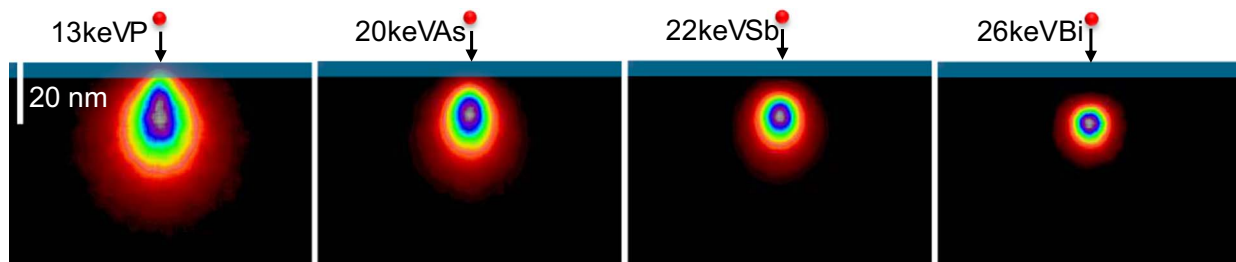

Fig. 1. Simulations based on the Stopping and Range of Ions in Matter (SRIM) Monte-Carlo model [27] showing the localisation precision limitation of ion straggling for a common 20 nm implantation depth. The maps represent the probability of the ion position at the end of range for a single ion impact coordinate. Effects from ion channelling were neglected.

channel [60–62]. This method is suitable for loading a single dopant atom into an otherwise undoped device and it is necessary to ensure the transistor structure can withstand the post-implant annealing step necessary to activate the implanted ion. Not all large-scale architectures may incorporate suitable transistors for application of this method.

2.2. Ion beam induced charge

To address the problem of process-flow compatible deterministic doping, we have developed a method that employs the signal generated by the induction of charge on surface detector electrodes following the dissipation of kinetic energy by ionization after ion impact [63]. This phenomenon is known as ion beam induced charge (IBIC). These electrodes are used only for the implantation step and can be optimised independently of the final quantum devices themselves. Briefly: the stopping of an implanted ion induces ionization (electron-hole pairs) as well as nuclear scattering. Electric fields in the substrate separate the electron-hole pairs and the signal is induced on the electrodes as a consequence. For convenience, the signal amplitude is expressed in energy units which represents the fraction of the initial ion kinetic energy that goes into the production of electron-hole pairs. Representative values are listed in Table 1. This method allows the counting of ion impacts provided the signal is above the noise threshold of the detector electrode structure and associated electronics which is presently about 1.5 keV. Further developments in our laboratory of our charge-sensitive electronics have reduced this to below 0.25 keV at room temperature. As shown in Table 1, this is sufficient to register the impacts of sub-10 keV phosphorus ions and hence is suitable for the construction of arrays in which the straggling is limited to below 10 nm.

When this method is used in conjunction with devices masked with one or two lithographically defined nanoapertures, it is possible to employ an unfocused ion beam to make single donor devices. It is also possible to make two donor devices at the cost of a 50% device yield. A simulation of the positioning precision possible for 14 keV P^+ implantation is shown in Fig. 2. Although the spacing of the two implanted ions will have large variations owing to straggling, tuning of surface

gates could nevertheless address individual sites and tune the site-to-site coupling.

3. Experimental

3.1. Silicon

The experimental results from a production run to fabricate counted two or more atom devices with this method is shown in Fig. 3. Here the surface mask contained two 15 nm diameter nanoapertures separated by 50 nm irradiated by a 14 keV P ion beam. The ions can only enter the substrate through the apertures and hence the irradiation continued until two ion implantation signals were recorded above the noise threshold of the on-chip detector electrodes and the associated charge-sensitive electronics. As shown in Fig. 3, two outcomes are possible: either one ion per aperture of both ions in a single aperture. Straggling will ensure the ions in the second case are in different locations and hence may be suitable for further applications. As also shown in Fig. 3, device 3 recorded two transients above the noise threshold, however one had the wrong time constant for an ion implantation event and was determined to arise from an acoustic transient in the laboratory. Hence the signal time constant can also be used as an additional discrimination factor to improve confidence in the method.

A further example of the production of a large number of devices is shown in Fig. 4. Here a chip was configured with many construction sites each equipped with independent detector electrodes and associated charge-sensitive electronics for the implant signals. With a pitch of 1.2 mm, it was readily possible to direct a collimated ion beam from an implanter onto each site in turn and deterministically implant 2, 4 or 5 atoms as shown in this example. Subsequent device processing involves annealing to repair lattice damage as well as the integration of nanocircuitry with reference to location markers for control of the implanted dopant atom.

For devices fabricated with more than two atoms it is necessary to have methods for localisation of each implanted ion to a specific site. High resolution focused beams can be produced in a focused ion beam system employing suitable eutectic alloys in a high brightness liquid metal ion source. In this way it is possible to focus 60 keV P^{2+} ions to a
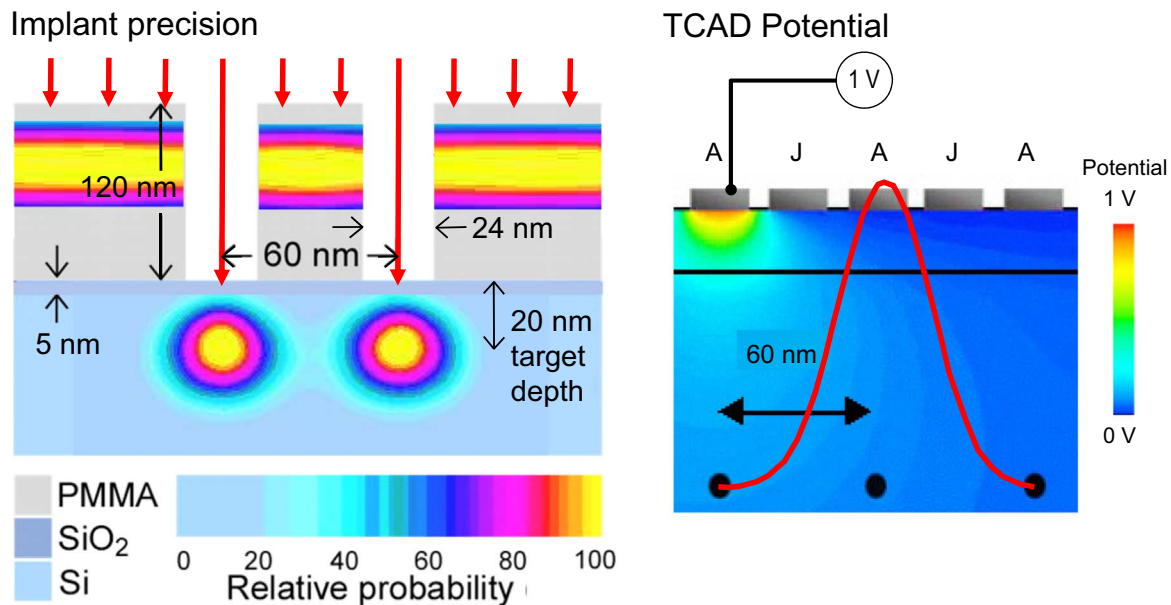

Fig. 2. Left – Ion end of range position probability map of a two atom device fabricated by implantation through two apertures in a PMMA surface mask based on SRIM simulations. The maps represent the probability based on randomly selected impact coordinates within the apertures for 15 keV P^+ ions. The silicon substrate has a prefabricated 5 nm thick gate oxide. Right – Technology Computer Aided Design (TCAD) simulations of the electric field profile within the substrate with the same configuration as the left diagram but configured now with A and J gates to control the individual donors and the inter-donor coupling. The red bell curve represents the probability distribution of ion spacings calculated from the coordinates portrayed in the left diagram.
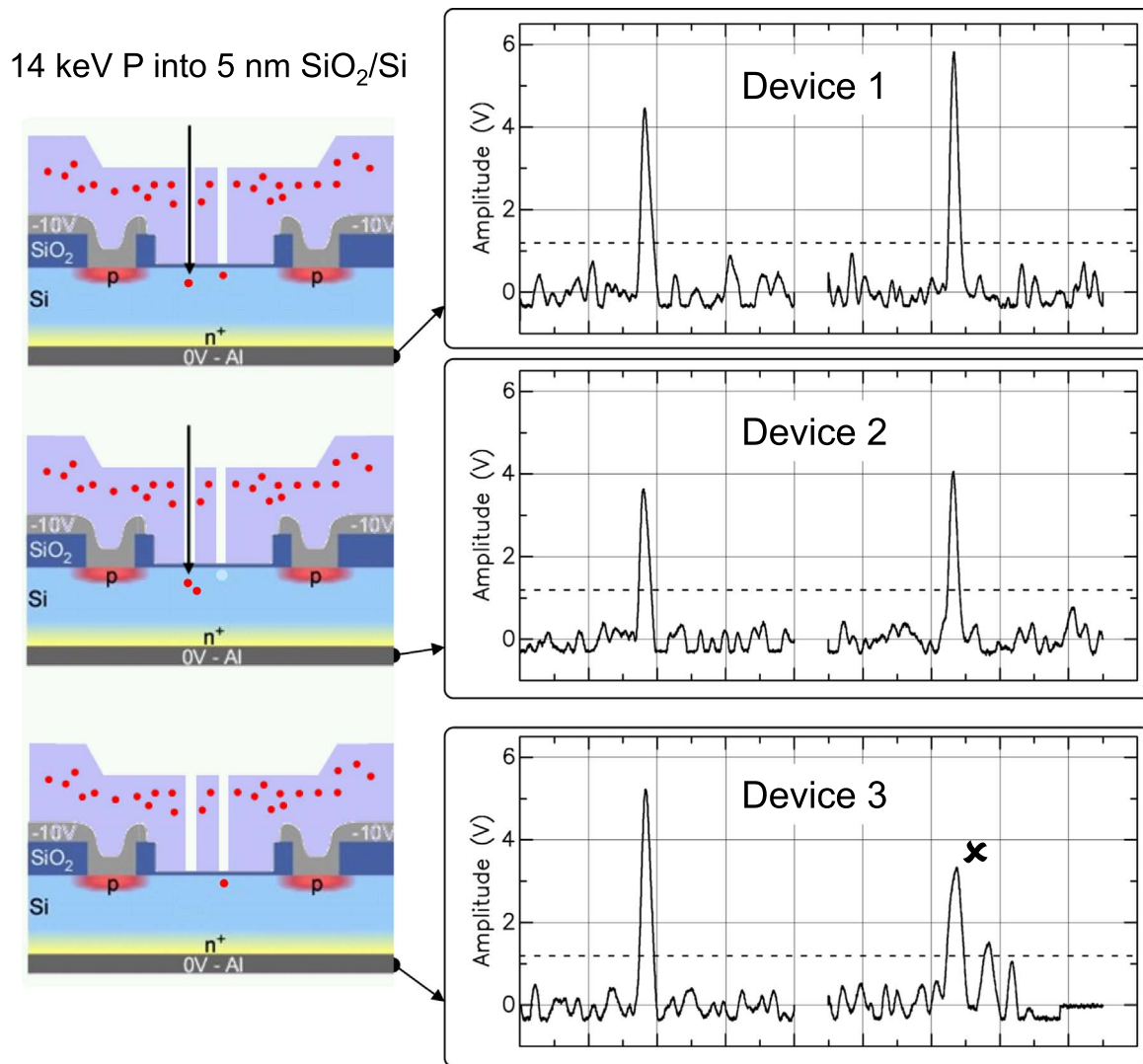
Fig. 3. Experimental ion implantation induced transient signals from 14 keV P+ ions incident through a PMMA surface mask into a silicon substrate configured with on-chip charge sensitive electrodes and associated processing electronics. The schematics for Device 1 and Device 2 show the two possible outcomes from two ions that produced the signals, however it is not possible to use the signals to determine the actual outcome. In the case of Device 3 the second signal was above the noise threshold shown by the dashed line but the time constant is indicative of the signal induced by an acoustic transient in the laboratory and hence the signal shape can be used to reject false signals. The major time step interval on the horizontal axis is 100 μs. See also Ref. [21] and [63].

localisation precision of 60 nm [56,57] and 120 keV Sb^{2+} ions to 30 nm [40]. It is likely that future developments of this technology will allow higher precision for the construction of large-scale arrays.

An alternative to high resolution focused beams is the use of an aperture in a nanostencil. This technique has attractive features because it imposes no special demands on the configuration of the ion source and hence works with a wide range of ions. Also for deterministic implantation the beam current needs to be low, commensurate with the time constant for the ion detection system. Around 1000 ions per second is adequate. A scanned nanostencil, used to collimate the beam from a ubiquitous gas plasma source can act as a repositionable implantation mask in this application. This method has been demonstrated by Schenkel et al. [64,65] who have also developed techniques for machining the collimating aperture in the nanostencil with a focused ion beam and back filling with platinum to achieve sub-20 nm apertures. Using this method, we have demonstrated a prototype system in which a sub-100 nm nanostencil is stepped across the substrate gated on the signal from the ion-implantation-induced electron–hole pairs [21]. Theoretical studies suggest this method could be developed to have sufficient precision to fabricate viable devices [66,67].

A practical demonstration of this method is shown in Fig. 5. Here the nanostencil consisted of a narrow slot milled in a silicon cantilever of an Atomic Force Microscope (AFM) backfilled with platinum to narrow the slot to 50 nm. A piezo positioning stage is then used to localise the cantilever over a PMMA masked silicon photodiode which acted as the substrate. Counted ion induced charge signals from the photodiode are used to advance the location of the cantilever. In this case the apparatus was configured to use ion scattering to measure the three dimensional profile of the milled slot in the nanostencil. Physical models can be used to model the transmitted ion energy spectrum to recover the profile which can then be used to assess the function of the nanostencil to localise the sub-20 keV ions [68] used for doping listed in Table 1. For the demonstration shown in Fig. 5a conventional Ortec 142 A preamplifier was coupled to the photodiode itself held at room temperature and 1.5 MeV He$^+$ ions were used so that sufficient electron–hole pairs (~400 k) would be available per ion strike to generate signals well above the noise threshold which was ~10 k electron-hole pairs for this configuration. The pattern created by stepping the nanostencil across the substrate was measured after development of the PMMA. These patterns were used as an additional measure along
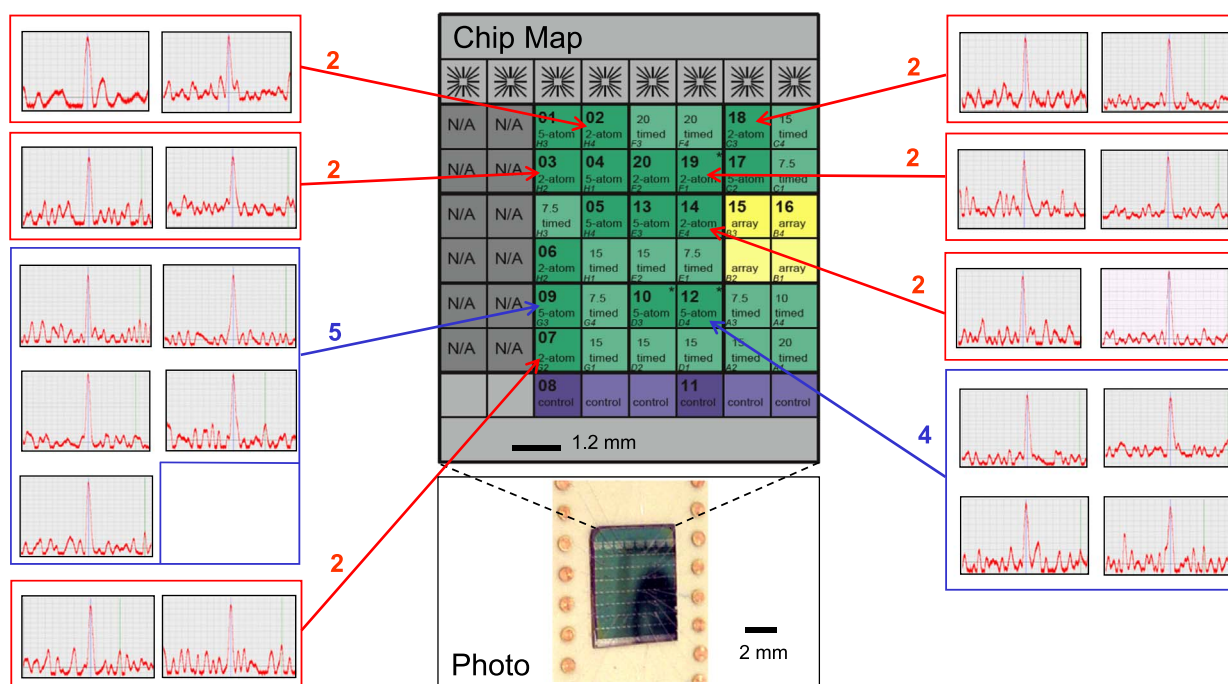
Fig. 4. Experimental ion implantation induced transient signals from the production of multiple deterministically ion implanted devices on a single chip where each device is configured with on-chip detector electrodes and associated charge-sensitive electronics. The photograph of the chip shows the mounting arrangement employing a high thermal conductivity ceramic package which is insensitive to piezoelectric effects. The chip was held close to the temperature of liquid nitrogen during the implantation and the ion beam was 14 keV P^+ with a beam diameter of 500 µm. The duration of the time window showing the transients is nominally 600 µs.
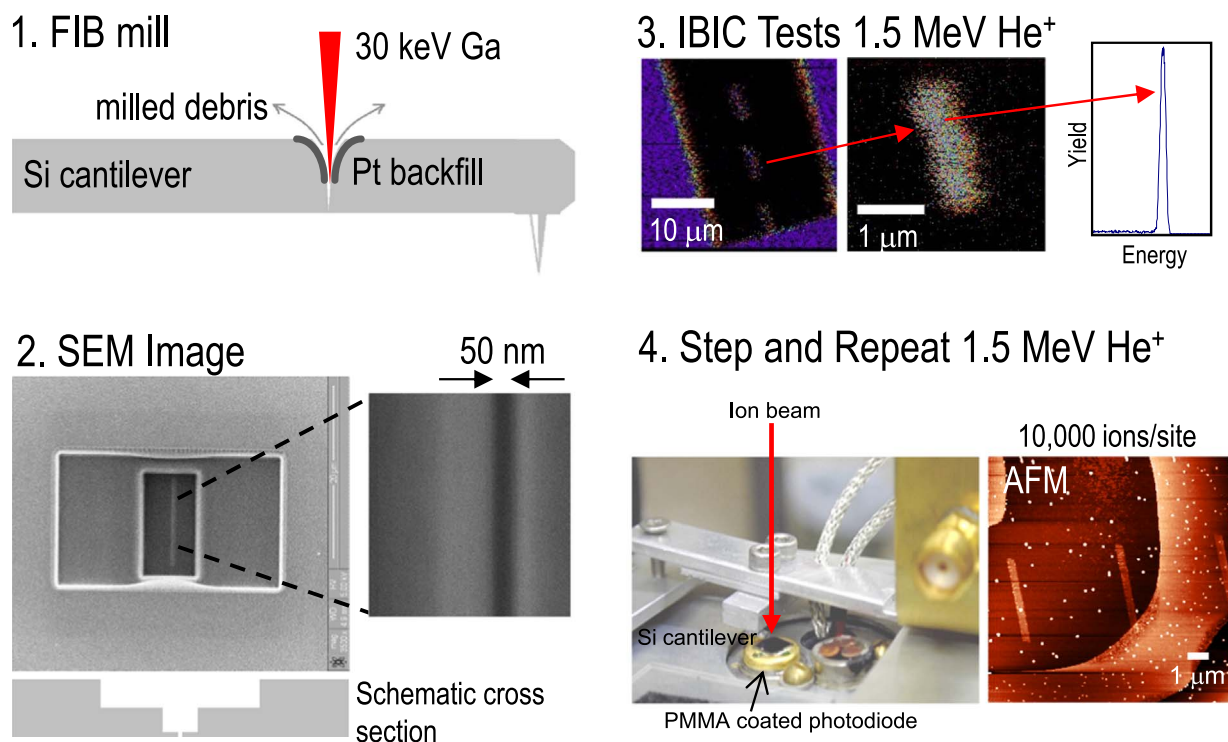

Fig. 5. The development of the process used to localise deterministic ion implants using a stepped nanostencil fabricated from an ion milled cantilever. 1: Drilling of the aperture using a focused 30 keV Ga ion beam and backfilling with Pt to narrow the aperture. 2: Measurement of the aperture, here configured as a narrow slot, using a scanning electron microscope (SEM). 3: Ion beam Induced Charge (IBIC) maps and associated energy spectrum of transmitted 1.5 MeV He^+ ions from which the three dimensional profile of the aperture can be determined. 4: Experimental configuration for the IBIC measurements where the energy spectrum of the transmitted ion beam is recorded by a pin diode at a scattering angle of 0°. The pin diode was coated with a thin film of PMMA that was much thinner than the ion range. Also shown is an AFM image of the replicas of the aperture recoded by the PMMA coated substrate. Adapted from reference [21].

with the transmitted ion energy spectrum to determine the internal structure of the collimator [68].

Improving this system with a higher precision sample stage and employing a cooled silicon substrate with low-capacitance on-chip detector electrodes leads to higher localisation precision [21]. In Fig. 6a nanostencil with a 90 nm diameter collimator and 14 keV Ar ions was stepped across the substrate gated on the ion impact signals from the detector electrodes. The silicon substrate was configured with a 200 nm
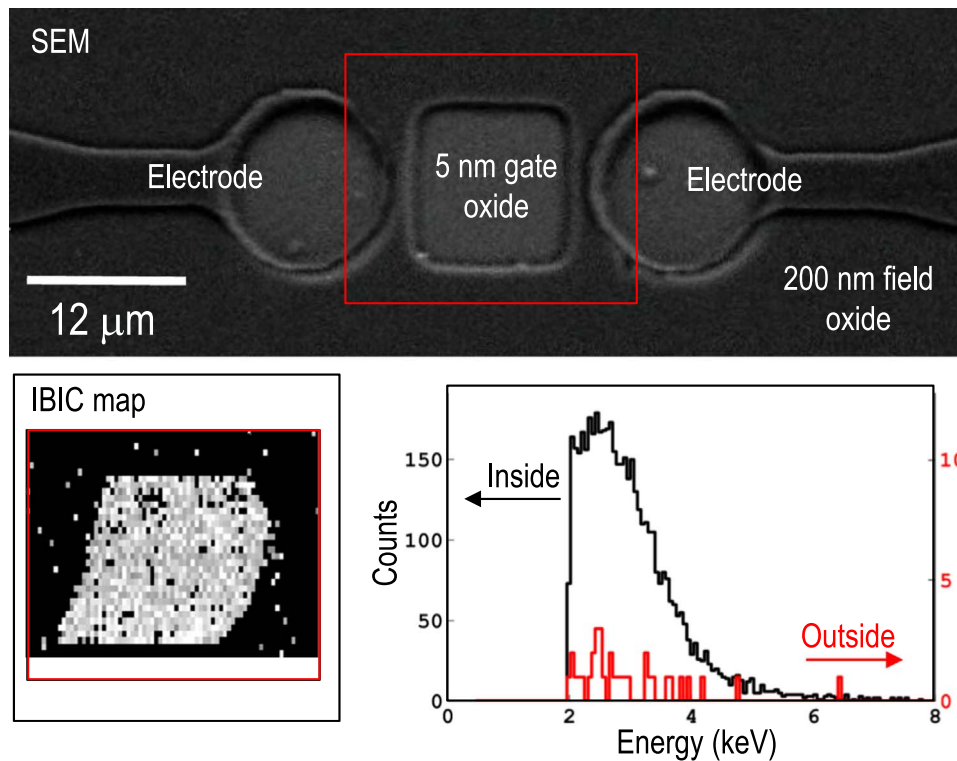
Fig. 6. Step-and-repeat IBIC map of the thin oxide region employing a scanned nanostencil configured with a 90 nm aperture and 14 keV Ar$^+$ ions. The nanostencil was advanced on either 6 ion impact signals from the on-chip electrodes and associated electronics, or 10 s of elapsed time. Ions that scatter into the thin oxide region while the stencil is positioned over the thick oxide region produced the signals where no ions are expected to penetrate into the silicon under the oxide. The histogram of ions from both regions are also shown with the low energy cut-off set at 2 keV. The number of scattered ions is in accord with theoretical simulations of ion scattering in the aperture and the geometry of the apparatus. Owing to thermal drift during the scan over the device, the IBIC map is distorted from the expected square shape. See text and reference [68] for more information.

thick field oxide surrounding a 12 µm square construction site with a nominally 5 nm thick gate oxide. The field oxide was thicker than the range of the incident ions so signals were only produced from ions that reached the silicon below the oxide in the construction region. The energy spectrum of scattered ions recorded by the on-chip electrodes is shown in Fig. 6. Under these conditions the ions entering the thin oxide layer are expected to have an energy peak at around 3.5 keV as observed. The energy spectrum of the ions detected while the nanostencil was positioned away from the thin oxide region arise from small angle scattering from the aperture in the cantilever which allows the ions to scatter into the thin oxide region. From theoretical models, it was concluded that the false-positive signal rate should be around 0.7% [68] which is consistent with the present result. Improvements in the physical geometry of the apparatus, by reducing the distance from the nanostencil to the substrate, can reduce these events to an acceptably low level.

3.2. Diamond

A further long-term goal is to adapt these silicon doping techniques for the high resolution placement of colour centres in diamond. For example the diamond negatively charged nitrogen-vacancy ($N - V^-$) centre [69] has many appealing features comparable to donors in silicon including long lived coherent states at room temperature and attributes for optical programming and read-out [70]. A diamond host lattice containing an engineered array of $N - V^-$ qubits in a monolithic quantum device [71] would be a robust and versatile platform for quantum information processing. With the recent availability of ultra-pure synthetic diamond our method could provide a potential pathway to combine for the first time high placement resolution with single ion detection and local processing for conversion of implanted nitrogen atoms to stable $N - V^-$ centres [72]. But there are formidable barriers

to be overcome in the construction of large-scale $N - V^-$ arrays in diamond with ion implantation along with the problem of fabricating large and complex structures in diamond with the same utility as is routine for silicon [73,74]. Also the conversion efficiency from a single deterministically implanted N ion into a suitable $N - V^-$ centre remains an unsolved problem with little progress to date. Although conversion efficiencies above 50% are reported for MeV N$^+$ implantation into diamond [75], the conversion efficiency drops to 26% for 30 keV N$^+$ [76] which reaches a depth of 30 nm with straggling of 11 nm.

Other colour centres may have favourable thermodynamic pathways that lead from an implanted ion to a useful colour centre with high conversion efficiency. With regard to deterministic ion implantation in diamond, it appears that the new device grade material will be suitable for the techniques described here because very high charge collection efficiency with high lateral uniformity is now possible in diamond devices configured with surface electrodes without the need for substrate doping as is required for silicon. Fig. 7 [77] shows IBIC maps measured with MeV ions for a laterally biased diamond device revealing 100% charge collection efficiency between the electrodes. It is likely that, with suitable matching charge-sensitive electronics, this result could also be extended into the sub-20 keV regime needed to place shallow colour centres controlled and coupled by surface electrodes.

4. Conclusion

Ion implanted silicon devices have demonstrated a remarkable range of controlled quantum phenomena, including a recent test of Bell's inequality [78] utilising the electron and nuclear spins of a single implanted ^{31}P atom. Although there are numerous technical challenges to building a large scale device [79–81] with an array of deterministically
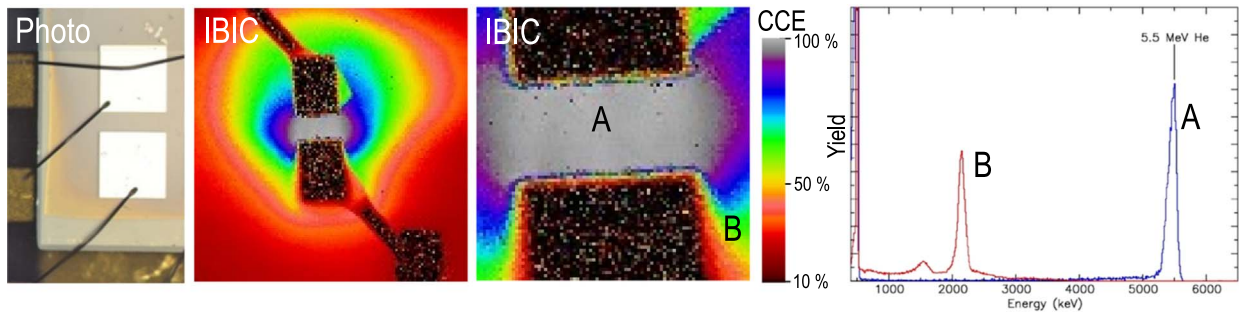
Fig. 7. From left: Photo micrograph of a high purity electronic grade diamond substrate configured with surface electrodes similar to the device examined here, IBIC image of a similar device, IBIC image of the 50 µm gap in the electrodes, IBIC spectra showing the pulse height spectra of the material in the gap (spectrum A) compared with the surroundings (spectrum B). The IBIC spectra show the efficiency is close to 100%. Beam was 5.5 MeV He$^+$ and bias voltage across the electrodes was 50 V. See reference [76] for more information.

implanted atoms, it is probable there will be a convergence of the localisation precision that can be achieved for sub-20 nm range ion implantation and the positioning tolerances required in new device architectures. As recognised in the 1986 review by Williams [84], ion implantation offers a measure of control which cannot be attained by more conventional processing methods and this attribute will extend the impact of ion implantation on solid state science and the new field of quantum technology. With more understanding of the thermodynamic pathways for the deterministic fabrication of diamond colour centres and further developments in improved techniques for localisation precision, deterministic doping by ion implantation has the potential to make the promise of quantum technology a practical reality.

Acknowledgments

References

[1] J.P. Dowling, G.J. Milburn, Quantum technology: the second quantum revolution, Philos. Trans. R. Soc. Lond. A 361 (2003) 1655–1674.
[2] D.P. DiVincenzo, The physical implementation of quantum computation, Fortschr. der Phys. – Prog. Phys. 48 (2000) 771–783.
[3] B.E. Kane, A silicon based quantum computer, Nature 393 (1998) 133–137.
[4] T.D. Ladd, F. Jelezko, R. Laflamme, Y. Nakamura, C. Munroe, J.L. O'Brien, Quantum computers, Nature 464 (2010) 45–53.
[5] N. Gisin, G. Ribordy, W. Tittel, H. Zbinden, Quantum cryptography, Rev. Mod. Phys. 74 (2002) 145–195.
[6] R. Blatt, C.F. Roos, Quantum simulations with trapped ions, Nat. Phys. 8 (2012) 277–284.
[7] A. Aspuru-Guzik, P. Walther, Photonic quantum simulators, Nat. Phys. 8 (2012) 285–291.
[8] V. Giovannetti, S. Lloyd, L. Maccone, Quantum Metrol, Phy. Res. Lab. 96 (2006) 010401.
[9] V. Giovannetti, S. Lloyd, L. Maccone, Quantum-enhanced measurements: beating the standard Quantum limit, Science 306 (2004) 1330–1336.
[10] L.P. McGuinness, Y. Yan, A. Stacey, D.A. Simpson, L.T. Hall, D. Maclaurin, S. Prawer, P. Mulvaney, J. Wrachtrup, F. Caruso, R.E. Scholten, L.C.L. Hollenberg, Quantum measurement and orientation tracking of fluorescent nanodiamonds inside living cells, Nat. Nanotechnol. 6 (2011) 358–363.
[11] M.W. Doherty, V.V. Struzhkin, D.A. Simpson, L.P. McGuinness, Y. Meng, A. Stacey, T.J. Karle, R.J. Hemley, N.B. Manson, L.C.L. Hollenberg, S. Prawer, Electronic

[12] properties and metrology applications of the diamond NV– center under pressure, Phys. Rev. Lett. 112 (047601) (2014) 1–5.
[13] P. Kómar, E.M. Kessler, M. Bishof, A.S. Sørensen, J. Ye, M.D. Lukin, A quantum network of clocks, Nat. Phys. 10 (2014) 582–587.
[14] J.P. Dowling, Quantum optical metrology - the lowdown on high-N00N states, Contemp. Phys. 49 (2008) 125–143.
[15] P. Hemmer, Closer to a quantum internet, Phys. 6 (2013) 62.
[16] F.A. Zwanenburg, A.S. Dzurak, A. Morello, M.Y. Simmons, L.C.L. Hollenberg, G. Klimeck, S. Rogge, S.N. Coppersmith, M.A. Eriksson, Silicon quantum electronics, Rev. Mod. Phys. 85 (2013) 961–1019.
[17] J.L. O'Brien, A. Furusawa, J. Vučković, Photonic quantum technologies, Nat. Photonics 3 (2009) 687–695.
[18] D.D. Awschalom, L.C. Bassett, A.S. Dzurak, E.L. Hu, J. Petta, Quantum spintronics: engineering and manipulating atom-Like spins in semiconductors, Science 229 (2013) 1174–1179.
[19] L.C.L. Hollenberg, A.S. Dzurak, C. Wellard, A.R. Hamilton, D.J. Reilly, G.J. Milburn, R.G. Clark, Charge-based quantum computing using single donors in semiconductors, Phys. Rev. B 69 (2004) 113301.
[20] S. Pezzagna, D. Rogalla, D. Wildanger, J. Meijer, A. Zaitsev, Creation and nature of optical centres in diamond for single-photon emission – overview and critical remarks, New J. Phys. 13 (2011) 035024.
[21] L. Rubin, J. Poate, Ion implantation in silicon technology, Ind. Phys. (2003) 12–15.
[22] J.A. van Donkelaar, C. Yang, A.D.C. Alves, J.C. McCallum, C.R. Hougaard, B.C. Johnson, F.E. Hudson, A.S. Dzurak, A. Morello, D. Spemann, D.N. Jamieson, Single atom devices by ion implantation, J. Phys. Cond. Mat. 27 (2015) 154204.
[23] C.C. Lo, C.D. Weis, J. van Tol, J. Bokor, T. Schenkel, All electrical nuclear spin polarization of donors in silicon, Phys. Rev. Lett. 110 (2013) 057601.
[24] J.J. Pla, K.Y. Tan, J.P. Dehollain, W.H. Lim, J.J.L. Morton, F.A. Zwanenburg, D.N. Jamieson, A.S. Dzurak, A. Morello, High-fidelity readout and control of a nuclear spin qubit in silicon, Nature 496 (2013) 334–338.
[25] J.J. Pla, K.Y. Tan, J.P. Dehollain, W.H. Lim, J.J.L. Morton, D.N. Jamieson, A.S. Dzurak, A. Morello, A single-atom electron spin qubit in silicon, Nature 489 (2012) 541–545.
[26] A. Morello, J.J. Pla, F.A. Zwanenburg, K.W. Chan, K.Y. Tan, H. Huebl, M. Möttönen, C.D. Nugroho, C. Yang, J.A. van Donkelaar, A.D.C. Alves, D.N. Jamieson, C.C. Escott, L.C.L. Hollenberg, R.G. Clark, A.S. Dzurak, Single-shot readout of an electron spin in silicon, Nature 467 (2010) 687–691.
[27] B. Koiller, X.D. Hu, S. Das Sarma, Electric-field driven donor-based charge qubits in semiconductors, Phys. Rev. B 73 (2006) 045319.
[28] J.F. Ziegler, M.D. Ziegler, J.P. Biersack, SRIM - The Stopping and Range of Ions in Matter (2010), Nucl. Instr. Methods B 268 (2010) 1818–1823.
[29] M. Naganawa, Y. Kawamura, Y. Shimizu, M. Uematsu, K.M. Itoh, H. Ito, M. Nakamura, H. Ishikawa, Y. Ohji, Accurate determination of the intrinsic diffusivities of boron, phosphorus, and arsenic in silicon: the influence of SiO$_2$ film, Jpn. J. Appl. Phys. 47 (2008) 6205.
[30] C.M. Yin, M. Rancic, G.G. deBoo, N. Stavria, J.C. McCallum, M.J. Sellars, S. Rogge, Optical addressing of an individual erbium ion in silicon, Nature 497 (2013) 91.
[31] C.D. Weis, C.C. Lo, V. Lang, A.M. Tyryshkin, R.E. George, K.M. Yu, J. Bokor, S.A. Lyon, J.J.L. Morton, T. Schenkel, Electrical activation and electron spin resonance measurements of implanted bismuth in isotopically enriched silicon-28, Appl. Phys. Lett. 100 (2012) 172104.
[32] G. Wolfowicz, A.M. Tyryshkin, R.E. George, H. Riemann, N.V. Abrosimov, P. Becker, H.J. Pohl, M.L.W. Thewalt, S.A. Lyons, J.J.L. Morton, Atomic clock transitions in silicon-based spin qubits, Nat. Nanotechnol. 8 (2013) 561.
[33] L.P. Kouwenhoven, T.H. Oosterkamp, M.W.S. Danoesastro, M. Eto, D.G. Austing, T. Honda, S. Tarucha, Excitation spectra of circular, few-electron quantum dots, Science 278 (1997) p1788–p1792.
[34] L.H. Willems van Beveren, H. Huebl, D.R. McCamey, T. Duty, A.J. Ferguson, R.G. Clark, M.S. Brandt, Broadband electrically detected magnetic resonance of phosphorus donors in a silicon field-effect transistor, Appl. Phys. Lett. 93 (2008) 072102.
[35] A. Morello, C.C. Escott, H. Huebl, L.H. Willems van Beveren, L.C.L. Hollenberg, D.N. Jamieson, A.S. Dzurak, R.G. Clark, Architecture for high-sensitivity single-shot readout and control of the electron spin of individual donors in silicon, Phys. Rev. B 80 (p081307(R)) (2009) 1–4.

[35] G. Mazzeo, E. Prati, M. Belli, G. Leti, S. Cocco, M. Fanciulli, F. Guagliardo, G. Ferrari, Charge dynamics of a single donor coupled to a few-electron quantum dot in silicon, Appl. Phys. Lett. 100 (2012) 213107.

[36] G.P. Lansbergen, R. Rahman, C.J. Wellard, I. Woo, J. Caro, N. Collaert, S. Biesemans, G. Klimeck, L.C.L. Hollenberg, S. Rogge, Gate-induced quantum-confinement transition of a single dopant atom in a silicon FinFET, Nat. Phys. 4 (2008) 656–661.

[37] M. Pierre, R. Wacquez, M. Vinet, O. Cueto, Single donor ionization energies in a nanoscale CMOS channel, Nat. Nanotechnol. 373 (2009) 1–5.

[38] M. Fernando Gonzalez-Zalba, D. Heiss, A.J. Ferguson, A hybrid double-dot in silicon, New J. Phys. 14 (2012) 023050.

[39] L.A. Tracy, T.M. Lu, N.C. Bishop, G.A. Ten Eyck, T. Pluym, J.R. Wendt, M.P. Lilly, M.S. Carroll, Electron spin lifetime of a single antimony donor in silicon, Appl. Phys. Lett. 103 (2013) 143115.

[40] M. Singh, J.L. Pacheco, D. Perry, E. Garratt, G. Ten Eyck, N.C. Bishop, J.R. Wendt, R.P. Manginell, J. Dominguez, T. Pluym, D.R. Luhman, E. Bielejec, M.P. Lilly, M.S. Carroll, Electrostatically defined silicon quantum dots with counted antimony donor implants, Appl. Phys. Lett. 108 (2016) 062101.

[41] D.R. McCamey, H. Huebl, M.S. Brandt, W.D. Hutchison, J.C. McCallum, R.G. Clark, A.R. Hamilton, Spin-dependent scattering off neutral antimony donors in Si field-effect transistors, Appl. Phys. Lett. 89 (2006) 182115.

[42] C.C. Lo, J. Bokor, T. Schenkel, J. He, A.M. Tyryshkin, S.A. Lyon, Spin-dependent scattering off neutral antimony donors in Si field-effect transistors, Appl. Phys. Lett. 91 (2007) 242106.

[43] A. Wallraff, D.I. Schuster, A. Blais, L. Frunzio, R.S. Huang, J. Majer, S. Kumar, S.M. Girvin, R.J. Schoelkopf, Strong coupling of a single photon to a super-conducting qubit using circuit quantum electrodynamics, Nature 431 (2004) 162–167.

[44] H. Wu, R.E. George, J.H. Wesenberg, K. Mølmer, D.I. Schuster, R.J. Schoelkopf, K.M. Itoh, A. Ardavan, J.J.L. Morton, G.A.D. Briggs, Storage of multiple coherent microwave excitations in an electron spin ensemble, Phys. Rev. Lett. 105 (2010) 140503.

[45] D.I. Schuster, A.P. Sears, E. Ginossar, L. DiCarlo, L. Frunzio, J.J.L. Morton, H. Wu, G.A.D. Briggs, B.B. Buckley, D.D. Awschalom, R.J. Schoelkopf, High-cooperativity coupling of electron-spin ensembles to superconducting cavities, Phys. Rev. Lett. 105 (2010) 140501.

[46] Y. Kubo, F. Ong, P. Bertet, D. Vion, V. Jacques, A. Dzhang, A. Dréau, J.F. Roch, A. Auffeves, F. Jelezko, J. Wrachtrup, M. Barthe, P. Bergonzo, D. Esteve, Strong coupling of a spin ensemble to a superconducting resonator, Phys. Rev. Lett. 105 (2010) 140502.

[47] Y. Kubo, C. Grezes, A. Dewes, T. Umeda, J. Isoya, H. Sumiya, N. Morishita, H. Abe, S. Onoda, T. Ohshima, V. Jacques, A. Dréau, J.F. Roch, I. Diniz, A. Auffeves, D. Vion, D. Esteve, P. Bertet, Hybrid Quantum Circuit with a Superconducting Qubit Coupled to a Spin Ensemble, Phys. Rev. Lett. 107 (2011) 220501.

[48] J. van der Heijden, J. Salfi, J.A. Mol, J. Verduijn, G.C. Tettamanzi, A.R. Hamilton, N. Collaert, S. Rogge, Probing the Spin States of a Single Acceptor Atom, Nano Lett. 14 (2014) 1492–1496.

[49] D. Moraru, A. Udhiarto, M. Anwar, R. Nowak, R. Jablonski, E. Hamid, J.C. Tarido, T. Mizuno, M. Tabe, Atom devices based on single dopants in silicon nanostructures, Nanoscale Res. Lett. 6 (2011) 479.

[50] J.O. Douglas, P.A.J. Bagot, B.C. Johnson, D.N. Jamieson, M.P. Moody, Optimisation of sample preparation and analysis conditions for atom probe tomography characterisation of low concentration surface species, Semicond. Sci. Technol. 31 (2016) 084004.

[51] W. Schnitzler, G. Jacob, R. Fickler, F. Schmidt-Kaler, K. Simger, Focusing a deterministic single-ion beam, New J. Phys. 12 (2010) 065023.

[52] G.Jacob, K.Groot-Berning, S.Wolf, S.Ulm, L.Couturier, U.Poschinger, F.Schmidt-Kaler, K.Singer, Single Particle Microscopy with Nanometer Resolution, ⟨http://arxiv.org/abs/1405.6480⟩.

[53] J.L. Hanssen, S.B. Hill, J. Orloff, J.J. McClelland, Magneto-optical-trap-based, high brightness ion source for use as a nanoscale probe, Nano Lett. 8 (2008) 2844–2850.

[54] B. Knuffman, A.V. Steele, J.J. McClelland, Cold atomic beam ion source for focused in beam applications, J. Appl. Phys. 114 (2013) 044303.

[55] G. Jacob, K. Groot-Berning, S. Wolf, S. Ulm, L. Couturier, S.T. Dawkins, U.G. Poschinger, F. Schmidt-Kaler, K. Singer, Transmission microscopy with nanometer resolution using a deterministic single ion source, Phys. Rev. Lett. 117 (2016) 043001.

[56] T. Shinada, S. Okamoto, T. Kobayashi, I. Ohdomari, Enhancing semiconductor device performance using, ordered dopant arrays, Nature 437 (2005) p1128–p1131.

[57] T. Shinada, T. Kurosawa, H. Nakayama, Y. Zhu, M. Hori, I. Ohdomari, A reliable method for the counting and control of single ions for single-dopant controlled devices, Nanotechnology 19 (2008) 345202.

[58] E. Prati, Single electron effects in silicon quantum devices, J. Nanopart. Res. 15 (2013) 1615.

[59] T.Schenkel, C.Weis, C.Lo, A.Persaud, I.Chakarov, D.Schneider, J.Bokor, Deterministic doping and the exploration of spin qubits, AIP Conference Proceedings 1640, 124, 2015.

[60] C.D. Weis, A. Schuh, A. Batra, A. Persaud, I.W. Rangelow, J. Bokor, C.C. Lo, S. Cabrini, D. Olynick, S. Duhey, T. Schenkel, Mapping of ion beam induced current changes in FinFETs, Nucl. Instr. Methods B 267 (2009) 1222.

[61] B.C. Johnson, G.C. Tettamanzi, A.D.C. Alves, S. Thompson, C. Yang, J. Verduijn, J.A. Mol, R. Wacquez, M. Vinet, S. Rogge, D.N. Jamieson, Drain current modulation in a nanoscale field-effect-transistor channel by single dopant implantation, Appl. Phys. Lett. 96 (2010) 264102.

[62] M. Ilg, C.D. Weis, J. Schwartz, A. Persaud, Q. Ji, C.C. Lo, J. Bokor, A. Hegyi, E. Guliyev, I.W. Rangelow, T. Schenkel, Improved single ion implantation with scanning probe alignment, J. Vac. Sci. Technol. B 30 (2012) 06FD04.

[63] D.N. Jamieson, C. Yang, T. Hopf, S.M. Hearne, C.I. Pakes, S. Prawer, M. Mitic, E. Gauja, S.E.S. Andresen, F.E. Hudson, A.S. Dzurak, R.G. Clark, Controlled shallow single-ion implantation in silicon using an active substrate for sub-20-keV ions, Appl. Phys. Lett. 86 (2005) 202101.

[64] A. Persaud, J.A. Liddle, T. Schenkel, J. Bokor, T. Ivanov, I.W. Rangelow, Ion implantation with scanning probe alignment, J. Vac. Sci. Technol. B 23 (2005) 2798–2800.

[65] J. Meijer, S. Pezzagna, T. Vogel, B. Burchard, H.H. Bukow, I.W. Rangelow, Y. Sarov, H. Wiggers, I. Pluemel, F. Jelezko, J. Wrachtrup, F. Schmidt-Kaler, W. Schnitzler, K. Singer, Towards the implanting of ions and positioning of nanoparticles with nm spatial resolution, Appl. Phys. A – Mater. Sci. Process. 91 (2008) 567–571.

[66] J.A. van Donkelaar, A.D. Greentree, A.D.C. Alves, L. Jong, L.C.L. Hollenberg, D.N. Jamieson, Top-down pathways to devices with few and single atoms placed to high precision, New J. Phys. 12 (2010) 065016.

[67] C.J. Wellard, L.C.L. Hollenberg, F. Parisoli, L. Kettle, H.-S. Goan, J.A.L. McIntosh, D.N. Jamieson, Electron exchange coupling for single donor solid-state spin qubits, Phys. Rev. B 68 (2003) (195209-1).

[68] A.D.C. Alves, J. Newnham, J.A. van Donkelaar, S. Rubanov, J.C. McCallum, D.N. Jamieson, Controlled deterministic implantation by nanostencil lithography at the limit of ion-aperture straggling, Nanotechnology 24 (2013) 145304.

[69] A.L. Falk, D.D. Awschalom, Spins charge ahead, Nat. Photonics 7 (2013) 510.

[70] V. Acosta, P. Hemmer, Nitrogen-vacancy centres, physics and applications, MRS Bull. 38 (2013) 127–167.

[71] D.M. Toyli, C.D. Weis, G.D. Fuchs, T. Schenkel, D.D. Awschalom, Chip-scale nanofabrication of single spins and spin arrays in diamond, NanoLetters 10 (2010) 3168.

[72] J. Schwartz, A. Aloni, D.F. Oglketree, T. Schenkel, Effects of low-energy electron irradiation on formation of nitrogen–vacancy centers in single-crystal diamond, New J. Phys. 14 (2012) 043024.

[73] E. Gibney, flawed to perfection, Nature 505 (2014) 472.

[74] C.A. McLellan, B.A. Myers, S. Kraemer, K. Ohno, D.D. Awschalom, A.C. Bleszynski Jayich, Patterned formation of highly coherent nitrogen-vacancy centers using a focused electron irradiation technique, Nano Lett. 16 (2016) 2450–2454.

[75] S. Pezzagna, B. Naydenov, F. Jelezko, J. Wrachtrup, J. Meijer, Creation efficiency of nitrogen-vacancy centres in diamond, New J. Phys. 12 (2010) 065017.

[76] B. Naydenov, F. Reinhard, A. Lämmle, V. Richter, R. Kalish, U.F.S. D'Haenens-Johansson, M. Newton, F. Jelezko, J. Wrachtrup, Increasing the coherence time of single electron spins in diamond by high temperature annealing, Appl. Phys. Lett. 97 (2010) 242511.

[77] J.A. Davis, K. Ganesan, D.A. Prokopovich, M. Petasecca, M.L.F. Lerch, D.N. Jamieson, A.B. Rosenfeld, A 3D lateral electrode structure for diamond based microdosimetry, Submitt. Appl. Phys. Lett. (2016).

[78] J.P. Dehollain, S. Simmons, J.T. Muhonen, R. Kalra, A. Laucht, F. Hudson, K.M. Itoh, D.N. Jamieson, J.C. McCallum, A.S. Dzurak, A. Morello, Bell's inequality violation with spins in silicon, Nat. Nanotechnol. 11 (2016) 242.

[79] P. Neumann, R. Kolesov, B. Naydenov, J. Beck, F. Rempp, M. Steiner, V. Jacques, G. Balasubramanian, M.L. Markham, D.J. Twitchen, S. Pezzagna, J. Meijer, J. Twamley, F. Jelezko, J. Wrachtrup, Quantum register based on coupled electron spins in a room-temperature solid, Nat. Phys. 6 (2010) 249–253.

[80] G. Tosi, F.A. Mohiyaddin, S.B. Tenberg, R. Rahman, G. Klimeck, A. Morello, Silicon quantum processor with robust long-distance qubit couplings, arXiv 1509 (2015) 08538.

[81] C.D. Hill, E. Peretz, S.J. Hile, M.G. House, M. Fuechsle, S. Rogge, M.Y. Simmons, L.C.L. Hollenberg, A surface code quantum computer in silicon, Sci. Adv. 1 (2015) e1500707.

[82] G.F. Knoll, Radiation Detection and Measurement, 3rd ed., Wiley, New York, 1999.

[83] C. Canali, E. Gatti, S.F. Kozlov, P.F. Manfredi, C. Manfredotti, F. Nava, A. Quirini, Electrical properties and performances of natural diamond nuclear radiation detectors, Nucl. Instr. Methods 160 (1979) 73–77.

[84] J.S. Williams, Materials modification with ion beams, Rep. Prog. Phys. 49 (1986) 491.